Urban Forestry & Urban Greening 12 (2013) 220–229

Contents lists available at SciVerse ScienceDirect

Urban Forestry & Urban Greening

journal homepage: www.elsevier.de/ufug

Multiparametric model of urban park cooling island

B. Vidrih, S. Medved*

University of Ljubljana, Faculty of Mechanical Engineering, Laboratory for sustainable technologies in buildings, Aškerčeva 6, 1000 Ljubljana, Slovenia

ARTICLE INFO

Article history:
Received 10 July 2012
Received in revised form
13 November 2012
Accepted 6 January 2013

Keywords:
Climate
CFD
Green space
Thermal response model
Trees

ABSTRACT

This paper presents a study of mitigation of the heat island effect in the built environment with urban (city) parks. The park cooling island (PCI) effect, considering park grass cover and trees' density and age, is determined for selected extreme summer days at various wind speeds under the optimum soil water conditions in the root zone based on an all-day quasi-stationary thermal response. PCI was determined numerically by coupling a CFD model of an urban park and quasi-steady state, two-zone thermal response boundary condition models of each park element. The boundary models are evaluated in form of multi-parameter approximation polynomials taking into account the sensible and latent heat transfer and the geometrical, optical and thermal properties of park elements. Three-dimensional CFD modelling was used for the determination of temperature, humidity and air velocity fields in an urban park with a size of 140 m × 140 m. Based on the comparison of the measured and numerically determined air temperatures in the tree crowns, we proved that the method of linking the models is adequate for temperature and flow condition modelling in the city park environment.

The results are presented in the form of local PCI as the difference between local air temperature in the pedestrian zone and the reference air temperature preceding the park. The study proved that it is possible to normalise the cooling effect using the specific dimensionless coefficient of leaf area (LAI_{sp}), which includes an approximation of the density of trees planted in the park and their size or age. It was found out that the cooling effect of the park is up to −4.8 °C at LAI_{sp}, equal to 3.16, which corresponds to a planting density of 45 trees per hectare, with an age of 50 years. It was also found that with the length of the park cooling effect change decreases. The optimal length of the park with a LAI_{sp} 3 is 130 m.

Introduction

Increased displacement of the natural environment with urbanised areas in previous decades has led to significant changes of local microclimate conditions. One such phenomenon is the urban heat island. In the literature, different predictions of urban heat island intensity can be found, from slight (low as 0.6 °C) to very extreme (up to 12 °C) (Yagüe et al., 1991; Saitoh et al., 1996; Kłysik and Fortuniak, 1999; Rosenzweig et al., 2005; Kolokotsa et al., 2009; Memon et al., 2009). The urban heat island effect increases energy consumption for cooling and causes lower thermal comfort in the indoor as well as in outdoor urban environments. The most effective measures for mitigation of the urban heat island effect are a reduction of solar radiation absorptivity by shading, urban environment elements with higher albedo, latent heat storage, and (above all) evaporative cooling with green surfaces (Taha, 1997; Herbert et al., 1998; Santamouris et al., 2011).

Based on previous research, one can conclude that the most effective measure to mitigate urban heat islands is the integration of green surfaces and parks in the urban environment. Manglani (2004) presented an experimental analysis of the cooling effect of trees. She found that the air temperature in the tree crowns is up to 3.8 °C lower than the surrounding air temperature in the daytime, while the temperature differences are minimal during night time. She stated that the surface temperature of leaves exposed to solar radiation is up to 4.1 °C higher than the temperature of unexposed leaves inside the crown. Vegetation and trees also influence the surface temperature of the build environment. If these are shaded, for example by tree crowns, their surface temperature is up to 19 °C lower compared to unshaded surfaces, while grass layer reduced maximum surface temperature by up to 24 °C (Armson et al., 2012). Onishi et al. (2010) found that the maximum reduction of surface temperature of individual parking lots could be up to 9.260 °C in summer by planting 30% trees and 70% grass.

An extensive experimental and numerical study of the influence of vegetation in urban areas was carried out by Shashua-Bar (Shashua-Bar and Hoffman, 2000; Shashua-Bar and Hoffman, 2002; Shashua-Bar et al., 2010). Based on the experimental measurements in green and other street canyons, the authors concluded that the heat island intensity is reduced up to 3.6 °C in urban areas with

* Corresponding author. Tel.: +386 1 4771 237; fax: +386 1 2518 56.
E-mail address: saso.medved@fs.uni-lj.si (S. Medved).

1618-8667/$ – see front matter © 2013 Elsevier GmbH. All rights reserved.
http://dx.doi.org/10.1016/j.ufug.2013.01.002

Nomenclature

A [m^2]	surface
a, b, c, d, e	constant
C	cloudiness factor
c_p [kJ/kgK]	specific heat
D [m]	zero plane displacement
D [m]	diameter
F	view factor between two surfaces
G [W/m^2]	solar radiation
H [m]	height of grass layer or tree crown
h [m]	height
k [/]	Von Kraman's constant
k [/]	the coefficient of weakening of radiation
L [°]	latitude
L [m]	length of park
LAI [m^2/m^2]	leaf area index
MRS [°C]	mean square error
$\dot{m}$ [kg/h]	mass flow
n [/]	number of
p [kPa], [Pa]	air pressure
PCI [°C]	park cooling island
Q [W]	heat flux
r [s/m]	resistance
r^2 [%]	r square
T [°C, K]	temperature
v [m/s]	wind velocity
x,y,z [m]	dimensions of park
z [m]	height of wind measure
z_o [m]	roughness length for momentum
ρ [kg/m^3]	density

Greek symbols

τ [/],[h]	transmission coefficient, time
φ [%]	relative humidity
ρ [/]	reflection coefficients
ρ [kg/m^3]	density
Δ [kPa/°C]	slope vapour pressure curve
γ [kPa/°C]	psychrometric constant
Δ [m, kPa]	difference
σ [W/m^{2}K^4]	Stefan–Boltzmann constant
R [°C/W]	thermal resistance
α [/]	absorption coefficient
α [/]	wind exponent
β [°]	inclined of surface
ε [/]	emissivity of surface

Subscripts

‘	actual vapour pressure
A	aerodynamic
Amb	ambient
B	boundary
C	convection, core
CFD	computational fluid dynamics
Cover	cover
ET	evaporation
Glob	global
Grass	grass layer
Ground	ground
i,j,k,l,m	indexes of surfaces
IR	long-wave radiation
MPM	multiple parametric model
Num	numerically calculated
Ref	reference
S	solar, surface,
S	stomatal, saturation vapour pressure
Sky	sky
Sp	specific
Tree	tree crown
TRL	test reference year

the placement of trees. The green area cooling effect depends significantly on the density and size of trees. By increasing the ground vegetation coverage from 10 to 70%, the cooling effect increases from 0.5 to 3.6 °C. Due to the increased latent heat flux by evapotranspiration, the average daily relative humidity is increased by about 12%.

Alexandri and Jones (2008) evaluated the impact of green surfaces for different locations around the world based on a two-dimensional numerical model of street canyon and meteorological data. They concluded that vegetation has the most significant influence in regions with dry and hot climates. In the case of greening the entire urban environment (ground and buildings), they predict a cooling effect between 6.6 °C and 9.1 °C, while in the case of greening only the building envelope, the cooling effect is halved. A lower cooling effect of vegetation is stated by Dimoudi and Nikolopoulou (2003). For an atrium of 18 m × 18 m, surrounded by buildings, they calculated that by planting trees the air temperature could reduced up to 0.8 °C.

Chen and Wong (2006) studied the local cooling effect of parks based on measurements of temperature in the park and surrounding areas, as well as the impact of parks on the neighbourhood. For an average value of leaf area index (LAI) of 3.8, they measured 1.8–2.3 °C lower air temperatures in the park of compared with air temperatures prior entering the park. Compared to the temperatures in the typical urban environment, these were lower by up to 8.2 °C. The park impact on the urban environment was evaluated based on numerical analysis, assuming a wind speed of 1.6 m/s in the direction of residential neighbourhoods. They found that air temperatures in the neighbourhood street canyons are lower by as much as 1.6 °C due to the park's cooling effect and that the influence can be felt in a distance equal to the length of the park.

Based on this literature review, we can conclude that city parks are important contributors to mitigating the urban heat islands effect, although the mentioned studies described only individual impacts of build environment elements, but not the effect of size, density and age of trees on the cooling effect of the park. In this paper, a parametric study of city park cooling potential is presented for a typical sunny day in the hottest summer month for the selected location (L 45.8°) regarding the density and size (age) of the trees, air temperature and wind velocity in open space before the city park.

Modelling of the cooling effect of city parks

In numerical modelling, we assume that parks consist of three elements: a grass layer, trees, and soil under the grass layer. For each element a thermal response model was developed in form of TRNSYS simulation tool TYPE (TRNSYS 16, 2005). In this way, transient conditions in the park were considered. Extreme daily temperatures of each node of park elements, as well as mass flow rate of the water vapour source were later used as boundary conditions in a steady state numerical solution of the temperature, velocity and humidity fields using the FLUENT CFD computer tool (FLUENT 13, 2008). The developing of the thermal response models and the method of incorporating this model into CFD modelling are presented in the next sections.

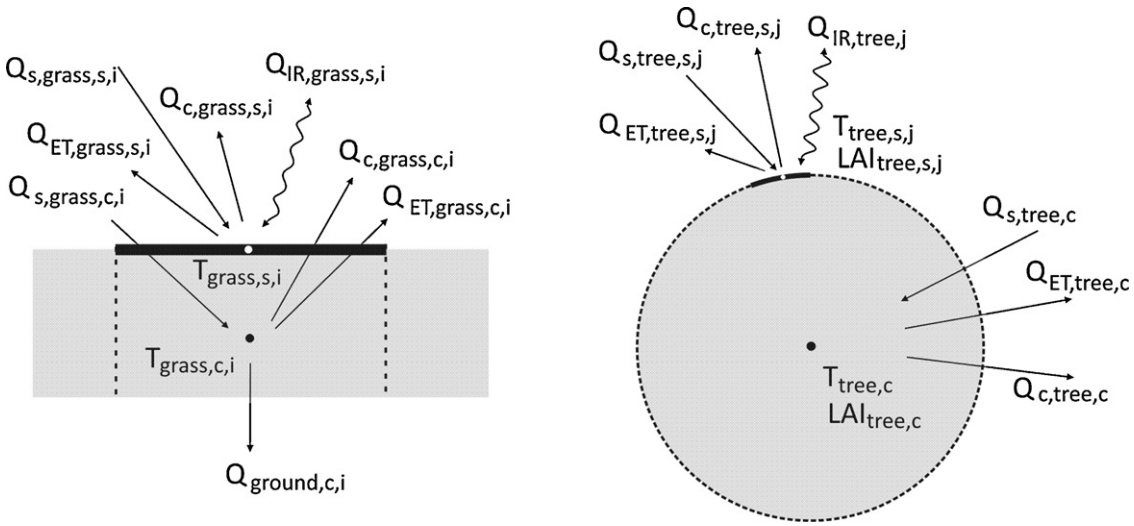

Fig. 1. Heat flows in the energy balance of grass and tree elements.

Thermal model of city park elements

The energy balance model was developed for each element of and urban park: the grass layer, the tree crowns and the soil layer; tree trunks are adiabatic and were considered only in the airflow model. For the grass layer and tree crowns, a two-zone model was used, consisting of a surface layer and a core node. Heat fluxes in energy balance models are presented in Fig. 1. The surface layer and the core of the grass are divided into *i* nodes, while the surface layer of the tree crown is divided into j nodes with only one core element. For each surface node, the absorbed solar radiation Q_S, longwave radiation Q_{IR}, convective Q_c and evaporative Q_{ET} heat fluxes are taken into account in the energy balance model. In addition to that, conductive heat fluxes between nodes $Q_{ground,c}$ were considered.

Absorbed solar radiation on the surface and in the core of i-th node of grass and j-th node of the tree crown surface layer and in the tree crown core depends on the leaves' absorbtivity α_s, the orientation of the surface segment and the reflection of solar radiation on all other surface layer nodes, which was determinated using view factors (Incropera and DeWitt, 1996). The ratio between absorbed solar radiation on the surface segment and in the core of element depends on leaf area index, which is calculated regarding to the total leaf area index LAI of those element. For grass, LAI_{grass} is equal to 1 (Allen et al., 2001), while for the tree crown, LAI_{tree} depends on the tree type and age, as shown in Fig. 2 (Peper et al., 2001; Linsen et al., 2005). In this study, the values for an elm tree were used.

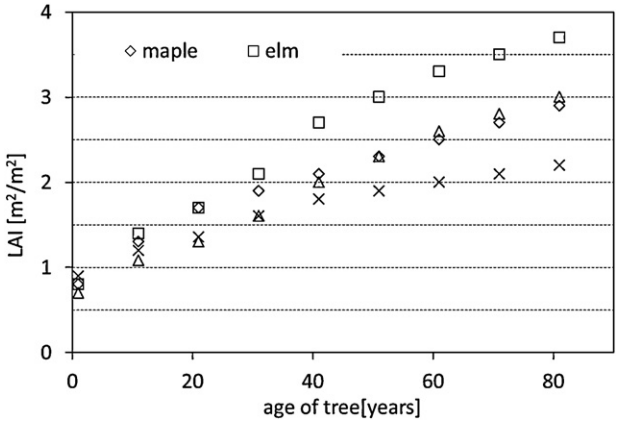

Fig. 2. LAI_{tree} for different tree species and their ages (Peper et al., 2001 and Linsen et al., 2005).

Surface and core leaf area index of grass layer is calculated by dividing of elements total leaf area index using Eq. (1) (Kjelgren and Montague, 1998):

$$LAI_{grass} = LAI_{grass,s} + LAI_{grass,c} \rightarrow LAI_{grass,c} = LAI_{grass} - LAI_{grass,s} = LAI_{grass} - \frac{1 - e^{-\tau \cdot LAI_{grass}}}{\tau} \quad (1)$$

In the same way, the surface and core leaf area indexes of the tree crowns were calculated. Transmissivity τ was set to 0.1 for grass layer (Allen et al., 2001), while for the trees it was calculated with Eq. (2) (Kjelgren and Montague, 1998):

$$\tau = e^{-\sigma \cdot LAI_{tree}} \quad (2)$$

where the σ is the coefficient of the weakening of the solar radiation. In our case, the value 0.85 was chosen in all cases (Kjelgren and Montague, 1998). The absorbed solar radiation on each grass layer node $Q_{s,grass,s,i}$ or tree crown surface node $Q_{s,tree,s,j}$ is calculated using Eqs. (3) and (4):

$$Q_{s,grass,s,i} = \left[\alpha_s \cdot A_i \cdot \left(G_{glob,\beta,i} + \rho_{s,tree} \cdot \sum_{k=1}^{o} \sum_{j=1}^{m} F_{i-j,k} \cdot G_{glob,\beta,j} \right) \right] \cdot \frac{LAI_{grass,s}}{LAI_{grass}} \quad (3)$$

$$Q_{s,tree,s,j} = \left[\alpha_s \cdot A_j \cdot \left(G_{glob,\beta,j} + \rho_{s,tree} \cdot \sum_{k=1}^{o} \sum_{j=1}^{m} F_{j-k,j} \cdot G_{glob,\beta,k,j} + \rho_{s,grass} \cdot \sum_{i=1}^{n} F_{j-i} \cdot G_{glob,\beta,i} \right) \right] \cdot \frac{LAI_{tree,s}}{LAI_{tree}} \quad (4)$$

where index *k* represents the number of the surround trees. The absorbed solar radiation in *i*-th grass core node is calculated by replacing the surface leaf area indexes $LAI_{grass,s}$ with core leaf area index $LAI_{grass,c}$ in Eq. (3). The absorbed solar radiation in core of the

k-th tree crown node is calculated using Eq. (5).

$$Q_{s,\mathrm{tree},c} = \left[\alpha_s \cdot \sum_{j=1}^{m} A_j \cdot \left(G_{\mathrm{glob},\beta,j} + \rho_{s,\mathrm{tree}} \cdot \sum_{k=1}^{o}\sum_{j=1}^{m} F_{j-k,j} \cdot G_{\mathrm{glob},\beta,k,j} + \rho_{s,\mathrm{grass}} \cdot \sum_{i=1}^{n} F_{j-i} \cdot G_{\mathrm{glob},\beta,i} \right)\right] \cdot \frac{\mathrm{LAI}_{\mathrm{tree},c}}{\mathrm{LAI}_{\mathrm{tree}}} \quad (5)$$

If any surface node is shaded by tree crown, the solar radiation on such surface is reduced by the transmissivity of the tree crown of the surrounding trees, calculated with Eq. (2).

Long-wave radiation heat transfer on each of i-th and j-th surface node $Q_{\mathrm{IR,grass},s,i}$ and $Q_{\mathrm{IR,tree},s,j}$ is calculated with the net heat transfer balance between park elements and the sky as differences between absorbed and emitted radiation, using Eqs. (6) and (7). The core of the elements does not exchange long wave radiation with the surroundings. In all cases, the emissivity of the long wave radiation of park elements $\varepsilon_{\mathrm{IR}}$ 0,96 was taken into account.

$$Q_{IR,\mathrm{grass},s,i} = \sigma \cdot A_i \left[F_{i-\mathrm{sky}} \cdot (\varepsilon_{IR} \cdot T^4_{\mathrm{grass},s,i} - \varepsilon_{IR,\mathrm{sky}} \cdot T^4_{\mathrm{sky}}) + \varepsilon_{IR} \cdot \sum_{k=1}^{o}\sum_{j=1}^{m} F_{i-k,j} \cdot (T^4_{\mathrm{grass},s,j} - T^4_{\mathrm{tree},s,k,j}) \right] \quad (6)$$

$$Q_{IR,\mathrm{tree},s,j} = \sigma \cdot A_j \left[F_{j-\mathrm{sky}} \cdot (\varepsilon_{\mathrm{IR}} \cdot T^4_{\mathrm{tree},s,j} - \varepsilon_{IR,\mathrm{sky}} \cdot T^4_{\mathrm{sky}}) + \varepsilon_{IR} \cdot \sum_{i=1}^{n} F_{j-i} \cdot (T^4_{\mathrm{tree},s,j} - T^4_{\mathrm{grass},s,i}) + \varepsilon_{IR} \cdot \sum_{k=1}^{o}\sum_{j=1}^{m} F_{j-k,j} \cdot (T^4_{\mathrm{tree},s,j} - T^4_{\mathrm{tree},s,k,j}) \right] \quad (7)$$

The sky temperature was determined with Eq. (8) (Martin and Berdahl, 1984):

$$T_{\mathrm{sky}} = T_{\mathrm{amb}} \cdot (\varepsilon_{IR,\mathrm{sky}} + 0.8 \cdot (1 - \varepsilon_{IR,\mathrm{sky}}) \cdot C_{cover})^{0.25} \quad (8)$$

where T_{amb} is the ambient air temperature and C_{cover} is the cloudiness factor of the sky. On a typical clear summer day, the value for C_{cover} is 0.1 and for $\varepsilon_{\mathrm{IR,sky}}$ is 0.9 (Martin and Berdahl, 1984). The convective heat flux of i-th grass surface layer node $Q_{\mathrm{c,grass},s,i}$ depends on aerodynamic resistant r_{a} and temperature difference (Eq. (9)):

$$Q_{c,\mathrm{grass},s,i} = \frac{c_p \cdot \rho}{r_a} \cdot (T_{\mathrm{grass},s,i} - T_{\mathrm{amb}}) \quad (9)$$

For all other surface layer nodes adequate nodes temperatures $T_{\mathrm{grass},c,i}$, $T_{\mathrm{tree},s,j}$ and $T_{\mathrm{tree},c}$ were used in Eq. (9).

Aerodynamic resistance r_a is evaluated with an expression that is derived from turbulent transfer and assuming a logarithmic wind profile as proposed by Yang and Friedl (2002):

$$r_a = \frac{\left(\frac{ln(z-d)}{z_o}\right)^2}{k^2 \cdot v_{\mathrm{amb},z}} \quad (10)$$

where d is zero plane displacement heigh, z_{o} is the rough length for momentum, k is the von Karman constant and v_{z} is wind speed at height z. To parameterise z_{o} and d for the grass layer and tree crown nodes, the second-order closure Yang model was used.

$$d = H \cdot \left[ln(1 + X^{1/6}) + 0.03 \cdot \ln(1 + X^6)\right] \quad (11)$$

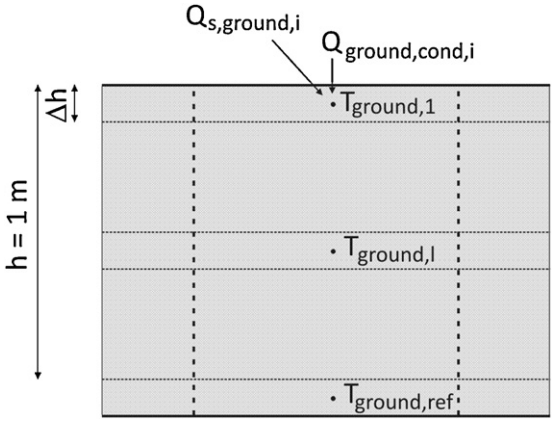

Fig. 3. Sub-layer of the soil beneath i-th grass core node.

$$z_o = 0.3 \cdot H \cdot (1 - d/H) \text{ for } 0.2 \le X \le 2 \quad (12)$$

where $X = 0.2 \cdot \mathrm{LAI}$ and H is the height of the grass layer or tree crown above the ground.

The evaporative heat flux for each of the grass nodes was calculated using the Penman_Monteith method (Allen et al., 2001). Eq. (13) was used for the grass surface layer node and Eq. (14) for the grass core node.

$$Q_{ET,\mathrm{grass},s,i} = \frac{\Delta \cdot (Q_{s,\mathrm{grass},s,i} - Q_{IR,\mathrm{grass},s,i}) + \frac{1}{A_i}\left(\rho \cdot c_p \cdot \frac{p_s - p'}{r_a}\right)}{\frac{1}{A_i} \cdot \left(\Delta + \gamma \cdot \left(1 + \frac{r_s}{r_a}\right)\right)} \quad (13)$$

$$Q_{ET,\mathrm{grass},c,i} = \frac{\Delta \cdot (Q_{s,\mathrm{grass},c,i} - Q_{\mathrm{ground},c,i}) + \frac{1}{A_i}\left(\rho \cdot c_p \cdot \frac{p_s - p'}{r_a}\right)}{\frac{1}{A_i} \cdot \left(\Delta + \gamma \cdot \left(1 + \frac{r_s}{r_a}\right)\right)} \quad (14)$$

Similarly, the evaporative heat flux on each tree node was calculated.

Stomatal resistance r_{s} 70 m/s was supposed for the grass layer, as proposed by Allen et al. (2001); it was determinate with the method proposed by Jarvis and McNaughton (as cited by Allen et al., 2001), using Eq. (15) (for trees standing alone):

$$\frac{r_s}{r_a} = 0.9 \cdot \frac{\Delta}{\gamma} + 0.9 \quad (15)$$

The conductive heat transfer between the grass layer core node and the soil was calculated using the meteorological data (ARSO, 2010) of soil temperature 1 m beneath the surface as reference temperature. The soil layer was divided into 10 sub-layers with equal depths of 0.1 m, as shown in Fig. 3.

A quasi-steady state energy balance was developed for first (Eq. (16)) and all the remaining soil sub-layers (Eq. (17)):

$$\rho_{\mathrm{ground}} \cdot c_{p,\mathrm{ground}} \cdot A_i \cdot \Delta h \cdot \frac{dT_{\mathrm{ground},1}}{d\tau} = Q_{s,\mathrm{ground},i} + Q_{\mathrm{ground,cond},i} - \frac{1}{R_{\mathrm{ground}}} \cdot (T_{\mathrm{ground},1} - T_{\mathrm{ground},2}) \quad (16)$$

$$\rho_{\mathrm{ground}} \cdot c_{p,\mathrm{ground}} \cdot A_i \cdot \Delta h \cdot \frac{dT_{\mathrm{ground},l}}{d\tau} = \frac{1}{R_{\mathrm{ground}}} \cdot (T_{\mathrm{ground},l-1} - T_{\mathrm{ground},l}) - \frac{1}{R_{\mathrm{ground}}} \cdot (T_{\mathrm{ground},l} - T_{\mathrm{ground},l+1}) \quad (17)$$

Table 1
Geometrical quantities of elm tree species that are used in presented study.

Age of tree (years)	Height of tree (m)	Height of crown (m)	Diameter of the crown (m)	Diameter of the stem (m)	LAI (/)
6	6.3	5.7	5.1	0.1	1.4
28	12.7	9.5	8.5	0.2	2.3
50	16.9	13.8	12.3	0.5	3.1

The absorbed solar radiation in the first i-th soil node is calculated with Eq. (18):

$$Q_{s,\text{ground},i} = A_i \cdot \left(G_{\text{glob},\beta,i} + \rho_{s,\text{tree}} \cdot \sum_{k=1}^{o} \sum_{j=1}^{m} F_{i-j,k} \cdot G_{\text{glob},\beta,j} \right) \cdot \tau_{\text{grass}} \tag{18}$$

The mass flow rate of water vapour from each of grass nodes and each tree is determined by the evaporative heat flux on all surface and core nodes using Eqs. (19) and (20):

$$\dot{m}_{\text{grass},i} = \frac{Q_{ET,\text{grass},s,i} + Q_{ET,\text{grass},c,i}}{r} \tag{19}$$

$$\dot{m}_{\text{tree}} = \frac{\sum_{j=1}^{m} Q_{ET,\text{tree},s,j} + Q_{ET,\text{tree},c}}{r} \tag{20}$$

Modelling of city park geometry

As assumed in this study, a city park consists of a grass layer and trees having different ages (sizes) and planting densities. Bjerke et al. (2006) concluded in their study that city parks improve microclimate urban conditions up to the tree age of 50 years. Regarding this, in our study, parks with 6, 28 and 50 year old trees and planting densities of 9, 21 and 45 trees per ha have been investigated. The largest selected tree planting density was determined on the basis of the ideal distribution of trees, by taking into account the geometric properties of the tree canopy at their maximum age. This ensures that tree crowns are not mutually intertwined. Table 1 presents the geometric features of elm tree species considered in the study.

To combine the age (size) and density of the trees in the park, the specific dimensionless leaf area index LAI_{sp} was introduced. It is determined with Eq. (21).

$$\text{LAI}_{sp} = \frac{A_{\text{grass}} \cdot \text{LAI}_{\text{grass}} + A_{\text{tree}} \cdot \text{LAI}_{\text{tree}} \cdot n_{\text{tree}}}{A_{\text{grass}}} \tag{21}$$

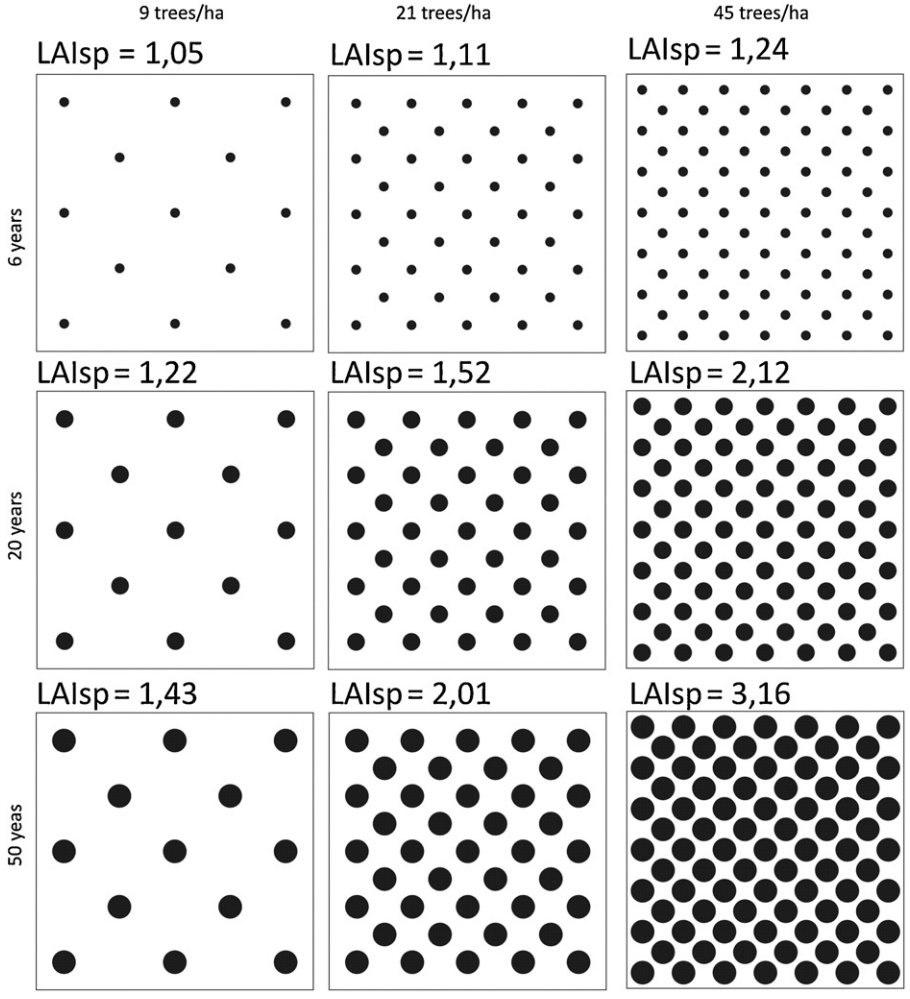

Fig. 4. Specific dimensionless leaf area index LAI_{sp} for different sizes and planting densities of the trees analysed in this study.

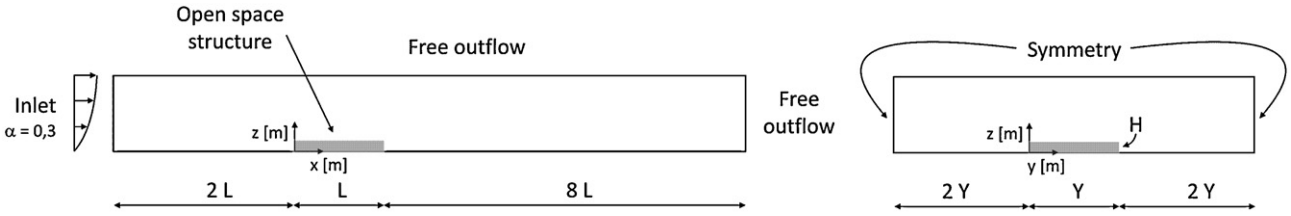

Fig. 5. Dimensions and boundary conditions used in CFD modelling; park, placed inside the domain, has size $L = Y = 140$ m, while H depends on size (age) of the trees.

The values of LAI_{sp} between 1.05 and 3.16 per m^2 of the park area were analysed as presented in Fig. 4.

CFD model

CFD modelling was performed for the parks having an area of 140 m × 140 m. The three-dimensional model is the based on the finite volume method solving the continuity, torque, energy and mass equations. Boussinesq's approximation was assumed and the 3D $k-\varepsilon$ Renormalisation Group turbulence model was chosen (RNG $k-e$ turbulence model) with the following constants: $C_1 = 1.44$, $C_2 = 1.92$, $C_\mu = 0.09$, $\sigma_k = 1$ and $\sigma_\varepsilon = 1.3$ (Robitu et al., 2006). Dimensions of the computational domain, shown in Fig. 5, were chosen in a way that minimises the influence of domain boundary conditions. The number of tetrahedral elements depends on the convergence criteria and the conditional provision of buoyancy-driven air movement around park elements (FLUENT, 2008). The number of cells ranged from 2,112,125 to 2,811,256.

The grass layer was modelled as a surface with the surface roughness z_o equal to 0.015 m. Tree crowns were modelled as a porous cylindrical body, while tree trunks were impermeable and adiabatic. The air permeability of the tree crown is determined based on the coefficient of pressure differences λ equal to 2.5 m^{-1} (Gromke, 2011).

Wind velocity profile at the CFD domain inlet was selected regarding to the typical conditions in urban environment with exponent α equal to 0.3. The kinetic energy profile and turbulent energy at inlet boundary were determined in a similar way.

Dynamic boundary conditions of city park elements

In the CFD modelling of the heat and mass transfer, the quasi-dynamic Dirichlet boundary conditions for heat transfer and the Neumann boundary condition for mass transfer were assumed. This means that the temperature and water vapour mass flow rate boundary condition were determined with hour-by-hour simulation of thermal response of each park element node in selected extreme summer day as results of the pre-selected range of influential variables: air temperature, humidity and velocity along each surface node. Solar radiation on each node is independent of local variables and therefore assumed as constant value. The range of influential variables is shown in Table 2. Such an approach enables the determination of the PCI of a city park, taking into account unsteady heat and mass transfer in park elements. This also means that boundary condition at each park element node is adapted to local temperature, velocity and humidity conditions.

The boundary surface temperature $T_{b,CFD}$ of each node was calculated as the average value of surface and core temperatures weighted by the surface and core leaf area index. Surface temperatures $T_{b,CFD}$ are then approximated by multi-parametric polynomials and used as adaptive boundary temperatures in CFD simulations. In this way, the thermal response models and CFD model are coupled and the boundary conditions are constantly adapted to the local temperature and velocity conditions at each air-surface boundary cell. The following expression of multi-parametric polynomials is used for node surface temperature approximation:

$$T_{b,CFD} = \sum_{i=1}^{4} (a_i + b_i \cdot T^i_{amb} + c_i \cdot v^i_{amb} + d_i \cdot \varphi^i_{amb} + e_i \cdot LAI^i) \qquad (22)$$

As an example, Table 3 presents values of the constants in Eq. (22). Because the determination of the PCI of city parks is the goal of this study, the constants in Table 3 were determined for extreme conditions during an extreme summer day for the selected location (L 45.08°, l 14.6°). The values of the leaf area index are presented above.

In a similar way, water vapour sources were determined per unit of area for the grass layer nodes and per volume unit for the trees for the tree crowns.

Verification of the thermal response models

The tree crown thermal response model was verified with in field measurements. A stand-alone 16 m tall tree with a crown diameter of 8 m was chosen for the experiment. The ambient temperature and wind velocity in open space before the tree, global solar radiation on horizontal plane and air temperatures inside the tree crown were measurement during six consecutive sunny summer days.

The ambient air temperature was measured with Ambient Air Temperature Sensor – TT_101_QR, the wind velocity and direction with Ekopower MAX 40 anemometer, global solar radiation was measured with a Kipp & Zonen type CM11-P pyranometer. Sensors were located in front of tree at the height of middle of the crown and connected to the datalogger unit Agilent 34970A capturing data every 300 s. The air temperature inside of the tree crown was measured with six wireless T-button temperature datalogger 22E with capturing data every 300 s. All six sensors were allocated evenly

Table 2
The range of influenced variables assumed in calculation of dynamic boundary condition for each surface node of park elements.

Influenced variable	range of influence variables
Ambient temperature	$T_{amb} = T_{amb,TRL} \begin{cases} +15^\circ C \\ -10^\circ C \end{cases}$; step = 5°C
Relative humidity	φ_{amb} = from 30 % to 80% ; step 10%
Wind velocity	v_{amb} = from 0.1 to 4.5 m/s; step 0.5 m/s

Table 3
The constants of multi-parametric polynomial for determination of surface nodes boundary temperature $T_{b,CFD}$.

Constants/i	1	2	3	4
a	−1.91	0	0	0
b	0.896	2.45e−3	−4.7e−4	3.9e−7
c	−0.97	7.7e−2	9.49e−3	−1.39e−3
d	0.0528	−1.58e−4	1.66e−6	−6.3e−9
e	−0.315	−3.155e−1	7.17e−2	7.2e−4

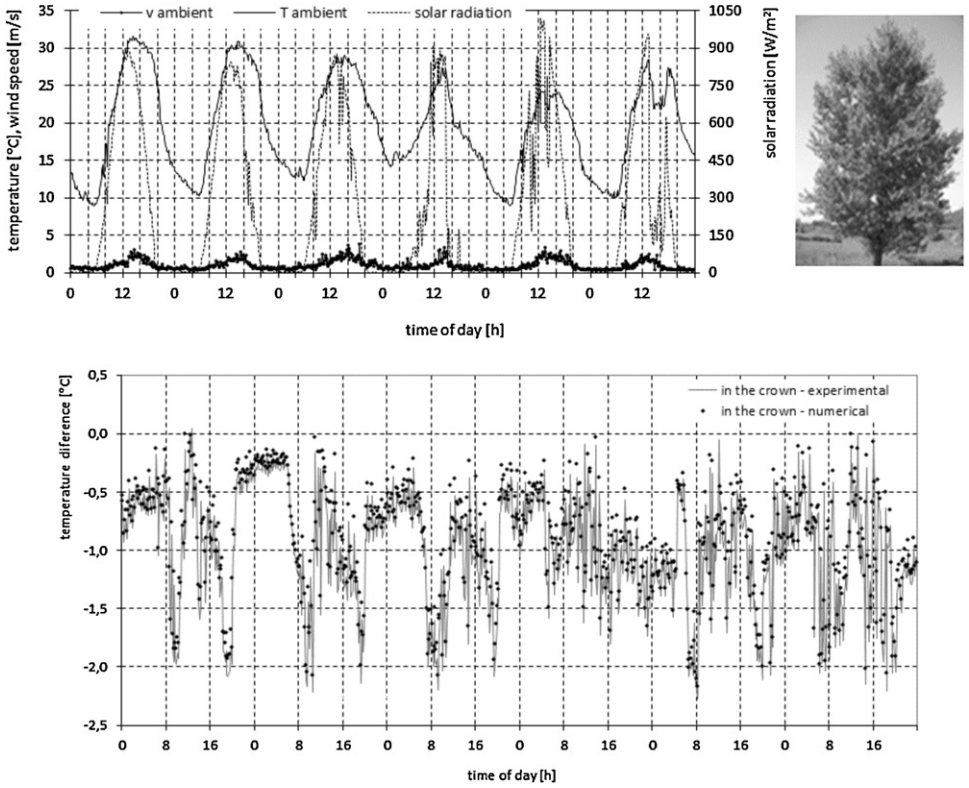

Fig. 6. Meteorological variables measured during the experiment (top) and comparison between measured and modelled average air temperatures inside the tree crown in a sunny summer day.

in the volume of the crown with no direct sun radiation. Average temperature of all six sensors was used as reference crown temperature and compared with numerical solution. Relative humidity as well as the rainfall was taken from the database of the nearby hydro-meteorological stations for the observed period. Optimum soil water content, needed for no stress evapotranspiration was assumed regarding to amount of precipitation in pre-measurement period.

A comparison of measured and calculated air temperatures in the tree crown is shown in Fig. 6, together with the meteorological conditions in the same period. The cooling effect of trees increases with the increase of solar radiation. The night-time cooling effect reaches an average value of −0.4 °C and in the daytime it is up to −2.1 °C. It can be concluded that numerical model is adequate, since the temperatures do not differ more than 0.2 °C at extreme conditions.

Results and discussion: The park cooling island

As presented in previous chapter, PCI is defined as the extreme difference between air temperature in the park and air temperature at park inlet boundary. Since the problem is transient, the thermal response of each park element was determined with an hour-by-hour simulation using meteorological variables from the local TRY database in hottest summer month (July, Ljubljana, Slovenia) (ARSO, 2010). The local time 15:00, the ambient air temperature at 28.5 °C, solar radiation on a horizontal plane 830 W/m^2 and relative air humidity of 48% define the reference boundary conditions at the moment of extreme air temperature conditions in the parks. As the wind speed in urban areas is highly random, we assumed that wind velocity varies in the range between 0.1 m/s (no wind) and 4.5 m/s. In all cases, it was assumed that the soil water condition in the root zone of the grass and the trees enables maximal evapotranspiration and therefore maximal cooling effect. Therefore the value of the water stress coefficient was taken 1 in all cases. As an example of the results of the CFD simulations, Fig. 7 shows the air temperature in the park at a reference height 1.2 m above the ground in the park having specific dimensionless leaf area index LAI_{sp} 3.16, velocity at the same high for the park having LAI_{sp} 1.52 and air relative humidity in the park having LAI_{sp} 1.05. All simulations were done for the reference boundary conditions.

From numerical simulations, it can be seen that local park cooling island increases with the length of the park, but can be assumed as constant though width of the park. Therefore, the park cooling island PCI inside the park was assumed as a one-dimensional variable, averaged on the plane of the pedestrian zone ($0.8 <= z <= 1.6$ m) and the width of the park ($0 <= Y <= 140$ m), using Eq. (23):

$$\mathrm{PCI}(x) = T(x) - T_{\mathrm{ref}} = \frac{\sum_{i=1}^{N} T_{(x,y,z),i} \cdot V_i}{\sum_{i=1}^{N} V_i} - T_{\mathrm{ref}} \quad (23)$$

where $0 <= x <= L$. N represents the number of numerical cells with a volume of V_i. Fig. 8 depicts the local park cooling island PCI (x) for different planting densities and ages of trees in the park. It can be seen that PCI (x) is significantly more dependent on the density and age of trees than the reference air velocity. The reason is that air velocity in the tree canopy is lowered and almost independent of the reference velocity $v_{o,\mathrm{ref}}$ and LAI_{sp}. The highest influence of the reference speed on PCI (x) occurs at $LAI_{sp} \sim 2$ as a result of more intensive air mixing of between trees canopies. For lower LAI_{sp} values, the distances between trees are larger, resulting in the occurrence of isolated flow in the leeward part of the canopy. In this case, PCI (x) increase almost linear through length of the park. At

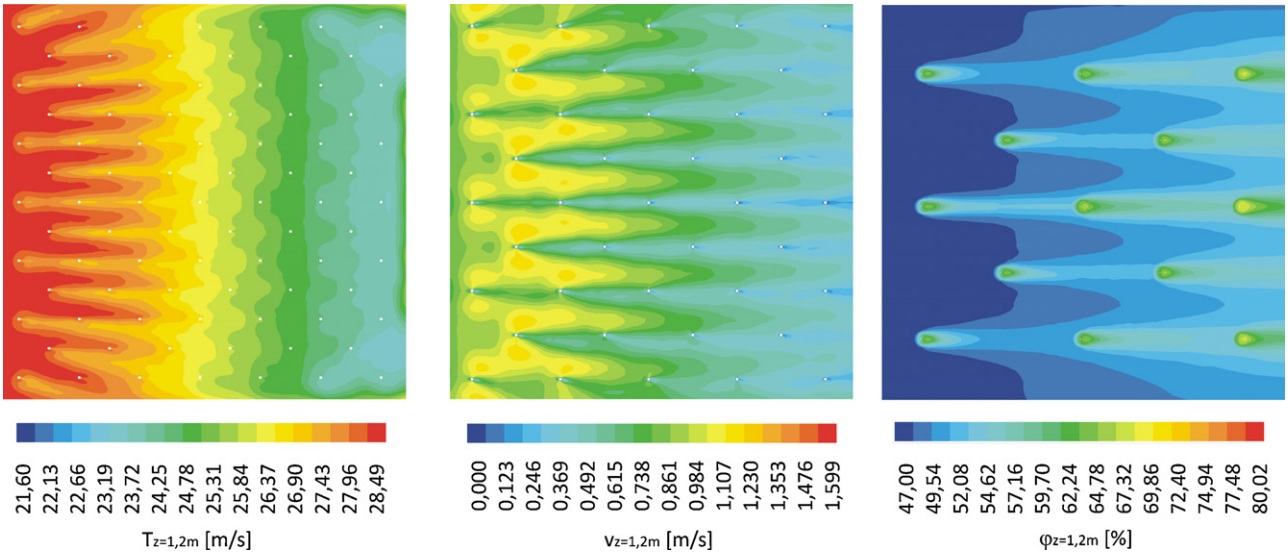

Fig. 7. Temperature at $z = 1.2$ m in the park having $LAI_{sp} = 3.16$ (left), velocity at $z = 1.2$ m in the park having LAI_{sp} 1.52 (middle) and relative air humidity in the park having $LAI_{sp} = 3.16$ (right), all simulation for $v_{amb,ref} = 1$ m/s.

higher planting densities, the trees' crowns are close together and evaporative cooling is less intense because of the lower permeability of the tree canopy. Because of that, the increasing of the PCI (x) become less significant though the end of the park.

The park cooling island PCI at the end of the park ($x = L$) is between −1.2 °C in the park having LAI_{sp} 1.05 and −4.7 °C in the park having LAI_{sp} 3.16. This corresponds to the park with 50-year-old trees and 45 trees per ha. In the parks with an LAI_{sp} larger than 3, the PCI reaches a maximum value towards end of the park, and this length of the park could be assumed as optimal one. Comparing to the park with a grass canopy only, it can be seen that the PCI is at least 4 °C greater if the specific dimensionless leaf area index LAI_{sp} is larger than 3. Because the reference velocity has quite a small effect of PCI, it was found that the park cooling island PCI

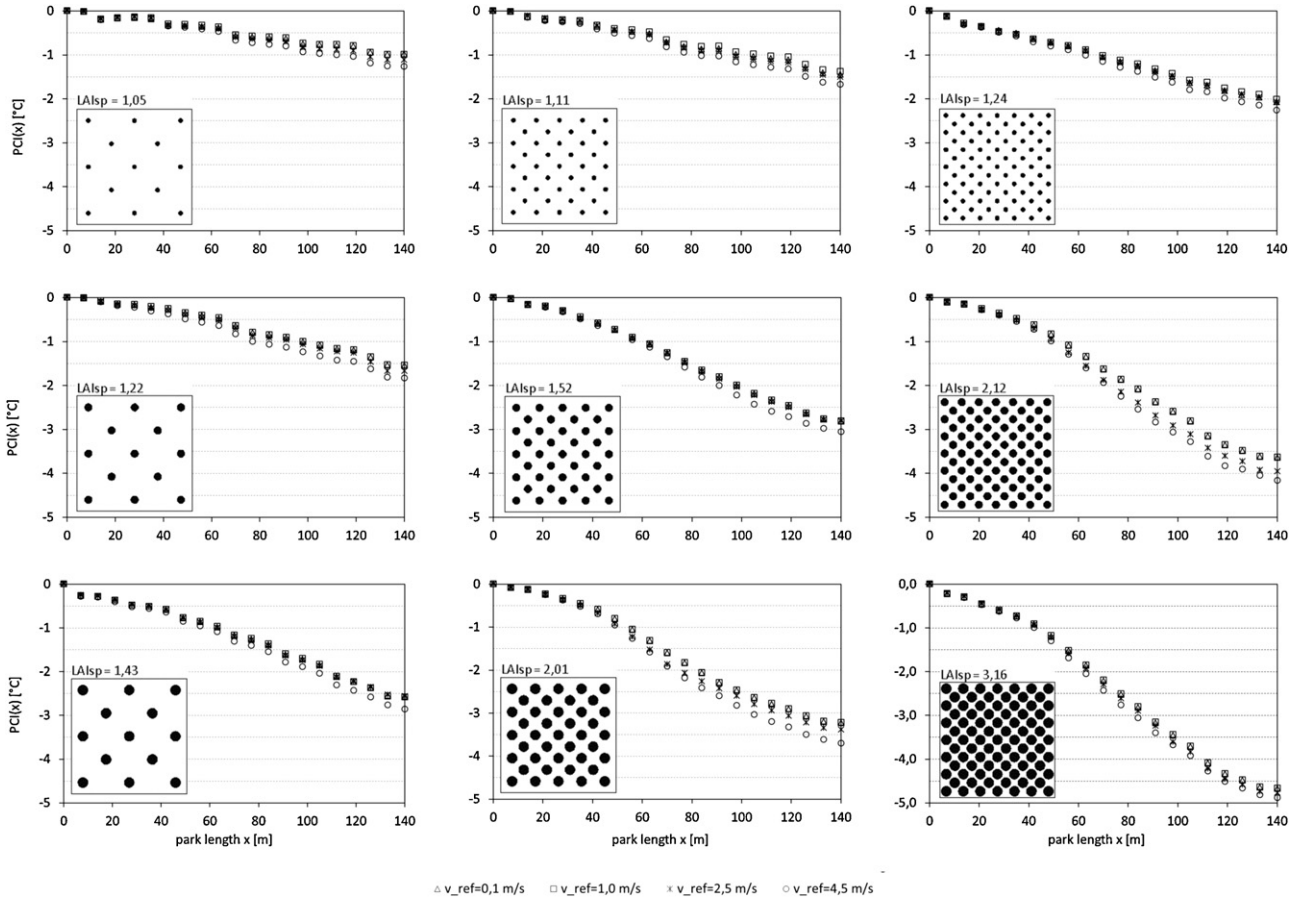

Fig. 8. The PCI (x) cooling effect along the park of different planting densities and age of trees.

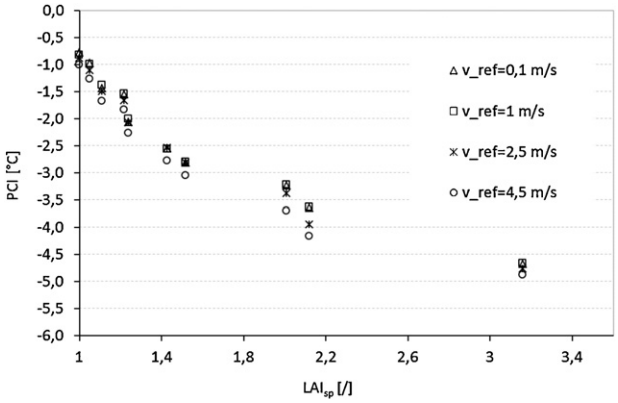

Fig. 9. The park cooling island PCI measured at the end of the park ($x = L = 140$ m) for parks with different specific dimensionless leaf area index LAI_{sp} and reference air velocities.

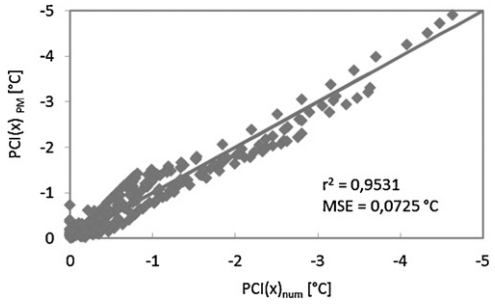

Fig. 10. Comparison between numerically (CFD) calculated PCI $(x)_{num}$ and PCI $(x)_{PM}$ calculated by parametric model presented in Eq. (24).

can be approximated as function of a specific dimensionless leaf area index LAI_{sp} as is presented in Fig. 9.

A parametric model for the local parks cooling island PCI (x) in the pedestrian zone was developed and presented in Eq. (24). Because of the low influence of the reference wind speed on PCI (x), the model can be used for any wind speed up to 4.5 m/s.

$$\mathrm{PCI}(x) = 0.27 + \mathrm{LAI}_{sp} \cdot (-0.32 + 7.1461 \times 10^{-3} \cdot x - 3.258 \times 10^{-4} \cdot x^2 + 1.869 \times 10^{-6} \cdot x^3 - 2.895 \times 10^{-9} \cdot x^4) \quad (24)$$

The parametric model was developed using Mathematica 6.0 (Mathematica 8.0, 2010). Different forms of the regression functions were compared with numerically calculated results on the basis of the coefficient of determination (r^2) and the mean square error (MSE). The regression functions with maximum values of r^2 and the minimum of the MSE were assumed to best fit the numerically calculated values. The parametric model is valid for x between 20 and 140 m. A comparison of PCI(x) of urban parks with LAI_{sp} up to 4 calculated with parametric model and from CFD simulations is presented on Fig. 10.

Conclusions

This paper presents a study on the cooling island potential of city parks expressed by the value of heat cooling island. A heat cooling island is defined the as temperature difference between average air temperature in pedestrian zone along the park and the reference air temperature prior to the park. A park area of 140 m × 140 m was chosen due to the fact that such area of the park corresponds with typical urban district. The heat cooling island potential was modelled by using thermal response models of park elements for the determination of space dependant boundary conditions of park elements in computer fluid dynamics modelling. In this way, the park cooling island was determined according to local conditions on the surface of park elements on a selected extreme summer day. In all cases optimum soil water conditions in the root zone enable no stress evapotranspiration was assumed. The method was verified by experiments and can be implemented for the modelling of urban heat islands and street canyon heat islands as well. A specific dimensionless leaf area index was introduced to analyse the total influence of the trees' density and age as the most influential park parameters. It was found out that city parks have significant potential in the mitigation of urban heat island. Despite the reduction of wind velocity inside the pedestrian zone, it was found out that reference wind velocity itself has minimum impact on the city park cooling islands.

References

Alexandri, E., Jones, P., 2008. Temperature decreases in an urban canyon due to green walls and green roofs in diverse climates. Building and Environment 43 (4), 480–493.
Allen, R.G., Pereira, L.S., Raes, D., Smith, M., 2001. Crop evapotranspiration (guidelines for computing crop water requirements), FAO Irrigation and Drainage Paper, No. 56. FAO, Utah, USA.
Armson, D., Stringer, P., Ennos, A.R., 2012. The effect of tree shade and grass on surface and globe temperatures in an urban area. Urban Forestry & Urban Greening 11 (3), 245–255.
ARSO, 2010. Test reference year for Ljubljana. Slovenian Environment Agency, Ljubljana.
Bjerke, T., Østdahl, T., Thrane, C., Strumse, E., 2006. Vegetation density of urban parks and perceived appropriateness for recreation. Urban Forestry & Urban Greening 5 (1), 35–44.
Chen, Y., Wong, N., 2006. Thermal benefits of city parks. Energy and Buildings 38 (2), 105–120.
Dimoudi, A., Nikolopoulou, M., 2003. Vegetation in the urban environment: microclimatic analysis and benefits. Energy and Buildings 35 (1), 69–76.
FLUENT 13, 2008. ANSYS Fluent. User Manual, http://www.ansys.com
Gromke, C., 2011. A vegetation modeling concept for Building and Environmental Aerodynamics wind tunnel tests and its application in pollutant dispersion studies. Environmental Pollution 159 (8–9), 2094–2099.
Herbert, J.M., Johnson, G.T., Arnfield, A.J., 1998. Modelling the thermal climate in city canyons. Environmental Modelling and Software 13 (3–4), 267–277.
Incropera, F.P., DeWitt, D.P., 1996. Fundamentals of Heat and Mass Transfer, fourth ed. John Wiley & Sons, New York.
Kjelgren, R., Montague, T., 1998. Urban tree transpiration over turf and asphalt surfaces. Atmospheric Environment 32 (1), 35–41.
Kłysik, K., Fortuniak, K., 1999. Temporal and spatial characteristics of the urban heat island of Łódź, Poland. Atmospheric Environment 33 (24–25), 3885–3895.
Kolokotsa, D., Psomas, A., Karapidakis, E., 2009. Urban heat island in southern Europe: the case study of Hania, Crete. Solar Energy 83 (10), 1871–1883.
Linsen, L., Karis, B.J., McPherson, E.G., Hamann, B., 2005. Tree growth visualization. The Journal of WSCG 12, 104–115.
Manglani, P., 2004. Radiative exchanges between a tree and a building surface. Phd thesis. Arizona State University, Phoenix, Arizona.
Martin, M., Berdahl, P., 1984. Characteristics of infrared sky radiation in the United States. Solar Energy 33 (3/4), 321–336.
Mathematica 8.0, 2010. Mathematica 8.0 for Microsoft Windows, 2010.
Memon, A.R., Dennis, Y.C., Leung, C.-H.L., 2009. An investigation of urban heat island intensity (UHII) as an indicator of urban heating. Atmospheric Research 94 (3), 491–500.
Onishi, A., Cao, X., Ito, T., Shi, F., Imura, H., 2010. Evaluating the potential for urban heat-island mitigation by greening parking lots. Urban Forestry & Urban Greening 9 (4), 323–332.
Peper, P.J., McPherson, E.G., Mori, S.M., 2001. Predictive equations for dimensions and leaf area of coastal Southern California street trees. Journal of Arboriculture 27, 169–180.
Robitu, M., Musy, M., Inard, C., Groleau, D., 2006. Modelling the influence of vegetation and water pond on urban microclimate. Solar Energy 80 (4), 435–447.
Rosenzweig, C., William, D.S., Parshall, L., Chopping, M., Pope, G., Goldberg, R., 2005. Characterizing the urban heat island in current and future climates in New Jersey. Global Environmental Change Part B: Environmental Hazards 6 (1), 51–62.
Saitoh, T.S., Shimada, T., Hoshi, H., 1996. Modeling and simulation of the Tokyo urban heat island. Atmospheric Environment 30 (20), 3431–3442.
Santamouris, M., Synnefa, A., Karlessi, T., 2011. Using advanced cool materials in the urban built environment to mitigate heat islands and improve thermal comfort conditions. Solar Energy 85 (12), 3085–3102.

Shashua-Bar, L., Hoffman, M.E., 2000. Vegetation as a climatic component in the design of an urban street: an empirical model for predicting the cooling effect of urban green areas with trees. Energy and Buildings 31 (3), 221–235.
Shashua-Bar, L., Hoffman, M.E., 2002. The Green CTTC model for predicting the air temperature in small urban wooded sites. Building and Environment 37 (12), 1279–1288.
Shashua-Bar, L., Tsiros, I.X., Hoffman, M.E., 2010. A modeling study for evaluating passive cooling scenarios in urban streets with trees. Case study: Athens, Greece. Building and Environment 45 (12), 2798–2807.
Taha, H., 1997. Urban climates and heat islands: albedo, evapotranspiration, and anthropogenic heat. Energy and Buildings 25 (2), 99–103.
TRNSYS 16, 2005. Transient System Simulation Tool. Solar Energy Laboratory, University of Wisconsin, Madison.
Yang, R., Friedl, M.A., 2002. Determination of roughness lengths for heat and momentum over Boreal Forests. Earth and Environmental Science. Boundary-Layer Meteorology 107 (3), 581–603.
Yagüe, C., Zurita, E., Martinez, A., 1991. Statistical analysis of the Madrid urban heat island. Atmospheric Environment Part B: Urban Atmosphere 36 (3), 327–332.